LAWRENCE
LIVERMORE
NATIONAL
LABORATORY

LLNL-JRNL-820189

Electrostatic Gating of Ion Transport in Carbon Nanotube Porins: A Modeling Study

Y. C. Yao, Z. Li, A. Gillen, M. Reed, A. Noy

March 4, 2021

Journal of Chemical Physics

Disclaimer

The Journal of Chemical Physics

LLNL-JRNL-820189

Electrostatic Gating of Ion Transport in Carbon Nanotube Porins: A Modeling Study

Yun-Chiao Yao[1,2], Zhongwu Li[1,3], Alice J. Gillen[1], Shari Yosinski[4], Mark A. Reed[4,5], Aleksandr Noy[1,2,a]

[1]Physical and Life Sciences Directorate, Lawrence Livermore National Laboratory, Livermore, California 94550, United States

[2]School of Natural Sciences, University of California Merced, Merced, California 95344, United States

[3]Jiangsu Key Laboratory for Design and Manufacture of Micro-Nano Biomedical Instruments, School of Mechanical Engineering, Southeast University, Nanjing 211189, China

[4]Department of Electrical Engineering, Yale University, New Haven, CT 06520, United States

[5]Department of Applied Physics, Yale University, New Haven, CT 06520, United States

Abstract

Carbon nanotube porins (CNTPs) are biomimetic membrane channels that demonstrate excellent biocompatibility and unique water and ion transport properties. Gating transport in CNTPs with external voltage could increase control over ion flow and selectivity. Herein, we used continuum modeling to probe the parameters that enable and further affect CNTP gating efficiency, including the size and composition of the supporting lipid membrane, slip flow in the carbon nanotube, and its intrinsic electronic properties. Our results show that the optimal gated CNTP device consists of a semiconducting CNTP inserted into a small membrane patch containing an internally conductive layer. Moreover, we demonstrate that the ionic transport modulated by gate voltages is controlled by the CNTP charge distribution along the tube under the external gate electric potential. The theoretical understanding developed in this study offers a valuable guide for the future design of gated CNTP devices for nanofluidic studies and the design of novel biomimetic membranes and cellular interfaces.

[a] Author to whom correspondence should be addressed: noy1@llnl.gov

Introduction

Efficient and controlled ion flow through nanoscale pores is critical for a variety of applications ranging from water desalination[1] to industrial separations[2, 3] and energy harvesting[4] to kidney dialysis.[5] An emerging body of nanofluidics research demonstrates that strong molecular level confinement in graphene nanoslits,[6, 7] carbon nanotubes,[8-12] 2D material nanopores,[13] and biological channels, such as aquaporins,[14] produces some of the highest known transport efficiencies.[15] Strong confinement in these nanostructures also induces a range of exotic behaviors including changes in water dielectric constant,[6] water phase transition temperatures,[16] and ionic conductance trends.[7, 10, 17-20] While nanofluidics researchers have been making significant progress in understanding and harnessing these phenomena,[15, 21] molecular confinement can offer other, and to date largely unexplored, opportunities to control and regulate transport in nanopores using applied external stimuli, such as electric fields or mechanical forces.[22, 23]

Membrane protein channels, such as aquaporins or Na^+ and K^+ channels in neurons,[24, 25] have elegant functionality that controls fluidic transport. Gated protein channels can switch between open and closed states to modulate ionic and molecular transport through the channel using membrane potential, ligand binding, mechanical force, temperature, or even light as their gating mechanism.[25] In voltage-gated ion channels in neurons, changes in the membrane potential modulate transmembrane ion current, enabling fast and reliable transmission of nerve signals over large distances.[25] Replicating such capabilities using synthetic analogs, such as single-digit nanopores[26] and other model nanofluidic systems,[27-29] has the potential to revolutionize biointerface technologies by enabling 'smart' membranes with increased efficiency and stability.

A number of microfluidic transistors and lab-on-chip devices have shown on/off behavior that is controlled by an externally applied gate voltage.[30-32] However, these devices have relatively large channel sizes and rely on ion-selective media to control the flow of ions and charged molecules,[33] which severely limits their application. Single-digit nanopores offer an opportunity to combine confinement and gating functionality to gain ultimate control over transport, perhaps down to a single ion level.

Previous work by our group has led to the development of carbon nanotube porins (CNTPs).[9, 34, 35] CNTPs are biomimetic channels made of single-walled carbon nanotubes,

which have well-defined diameters at the nanometer and sub-nanometer range. Furthermore, CNTPs can be coated with lipid molecules that disperse the CNTPs and enable their easy self-insertion into lipid membranes.[34, 35] Our previous studies showed efficient electrophoretic and electroosmotic transport in individual small diameter CNTPs incorporated into a modified planar lipid bilayer device, where lipid bilayers span over a ca. 100 nm diameter SiN_x aperture.[9, 20] This experimental configuration provides several advantages for exploring electrostatic gating of nanofluidic transport. Small diameter CNTPs provide strong confinement that is essential for efficient gating at higher ionic strength solutions. Moreover, carbon nanotubes with different pore sizes and electronic properties can be incorporated into the lipid bilayer, while the microfabricated SiN_x device platform allows reasonably simple incorporation of electrodes and straightforward ion current measurements increasing the versatility of the system.

Here we use continuum COMSOL modeling to explore the possibilities of creating gated CNTP devices and the basic parameters that govern their function. We demonstrate that we should be able to achieve efficient gating of CNTP channels and examine the impact of lipid size and composition to identify threshold requirements for gating. Using the optimal lipid configuration, we further probe the dependence of device gating on the intrinsic properties of the CNTPs, including slip length and permittivity. We believe that these results can be used to guide experimental approaches for creating gated CNTP devices and also inform the broader design space for the next generation of nanofluidic systems.

Simulations setup

To explore the possibility of constructing a gated CNTP device we started with the experimental setup that we developed for measuring ion conductance of individual CNTPs[9, 20] (Fig. 1A) and modeled it in the finite element analysis software COMSOL Multiphysics 5.5.[29] Our simulations used three physics modules for describing the processes in this system: electrostatic, transport of diluted species, and creeping flow, which are described by the Poisson equation, Nernst-Planck equation, and Stokes equation, respectively.[29, 36] We modeled the device as an axisymmetric cell (see Fig 1B and C for a cross-section and a three-dimensional (3D) model) that has two reservoirs with 50 nm

height and radius (r). These chambers were separated by a circular patch of a lipid membrane with a CNTP channel placed in the center. The parameters of the CNTP channel were matched to values obtained from previous experiments:[34] a length of 10 nm, radius of 0.58 nm, and CNT wall thickness of 0.34 nm, giving 1.5 nm as the carbon-to-carbon diameter of the CNTP.[8, 20, 34] The CNTP channel was also assigned an entrance charge density ($4e^-$), equivalent to four negatively charged functional groups at one end, that was distributed homogenously along the CNTP pore mouth. This value was chosen based on our best estimate of the number of COOH groups at the nanotube pore mouth.[20] The membrane matrix holding the CNTP was modeled as a 10 nm thick simplified lipid bilayer that was impermeable to liquid solutions. This lipid bilayer was divided into three parts: two hydrophilic outer layers and an inner hydrophobic layer. Both reservoirs were filled with 100 mM KCl solution (unless otherwise specified).

The bottom reservoir was grounded (0 V) and an external potential (V_p) was applied at the upper boundary of the top reservoir to drive the ion transport through the CNTP. To simulate the electrostatic gating of the device we have also incorporated a gating electrode into the device aperture rim,[37] with a gate voltage (V_g) applied at the boundary of the hydrophobic part of the lipid and the SiN_x aperture. The applied voltages varied across a bio-compatible range of -0.5 V and 0.5 V. Prior experiments showed that lipid bilayers spanning over the nanopores remained stable at these voltages.[38, 39] Ionic current was determined by integrating the current density of ions passing through a channel cross-section halfway along the CNTP. Currents at positions 1/3 and 2/3 along the CNTP were also checked to confirm the accuracy of the finite element modeling. In order to compare the gating efficiency of our system, we also calculated the gating factor as:

$$Gating\ Factor = I_{max}/I_{min}$$

where I_{max} and I_{min} were, respectively, the highest and lowest currents obtained at constant V_p and different applied gate voltages, V_g.

Device geometry, lipid configuration, and gating efficiency

We first investigated the ionic conductance and selectivity of the CNTP channel in the absence of an applied gate voltage (V_g = 0 V). In agreement with previous data from the literature,[17, 20, 28] we assigned a small negative charge to the inner surface of CNTP and

set the slip length to 1 nm at 100 mM KCl (additional details on the parameters used in the model are included in the Methods and Supplementary Table S1). As expected, the ion concentration distribution showed cation accumulation next to the negatively charged nanotube entrances (Fig. 1C, inset). A comparison of the cation and anion concentrations inside the channel indicated the channel was cation selective and the current-voltage (I- V_p) curves were linear within the +/- 0.5 V applied potential range (Fig. 1D), both in line with experimental observaions.[20] The conductance, 228 pS, and cation/anion ratio, ca. 14, also showed excellent agreement with previous experimental data obtained under similar conditions (214 ± 40 pS and ca. 12 at a KCl concentration of 100 mM),[20] indicating that our COMSOL model can effectively capture the major features of ion transport in 1.5 nm diameter CNTPs. Upon application of a gate voltage, however, this device configuration showed no gating effect as the current remained virtually constant with varying V_g (Fig. 1E). This behavior was not surprising because the lipid molecules are not very polarizable and thus acted as an insulator between the CNTP channel and the gate electrode, hindering electric field propagation.

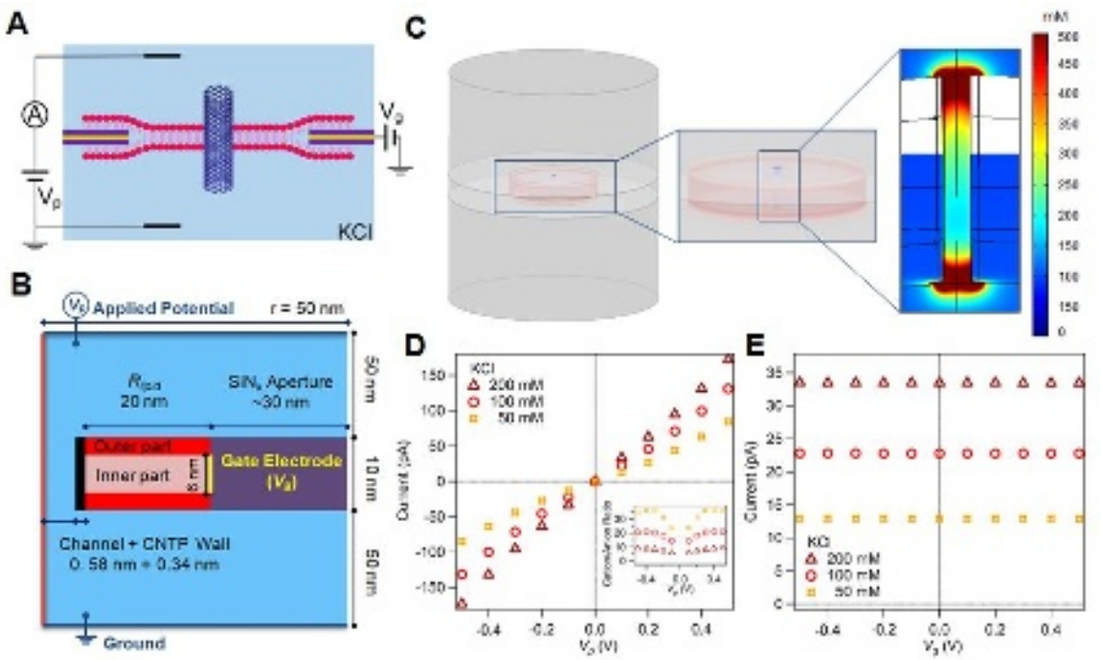

Figure 1. Gated CNTP device setup and initial conductance characteristics. (**A**) Schematics of the device setup. (**B**) The axisymmetric cross-section of the CNTP model. The applied potential (V_p) at the upper boundary of top reservoir drives the ionic current through the nanotube pore and the gate voltage (V_g) at the

boundary between lipid inner part and the SiNx aperture provides the applied gate voltage potential. (**C**) The 3D structure of the axisymmetric setup with zoomed-in view at the lipid patch and gate electrode rim. Inset: K^+ ion distribution along the CNTP channel at V_p = 0.1 V. (**D**) I-V_p curves for CNTP at 50, 100, and 200 mM KCl. Inset: Ionic current ratio of K^+ and Cl^- ions. (**E**) Ionic current of CNTP channel as a function of gate voltage in KCl solutions of different concentrations at V_p = 0.1 V.

One way to improve the gating efficiency would be to reduce the size of the bilayer patch, thus bringing the electrode closer to the CNTP channel. To test this hypothesis, we simulated transport in the devices with different SiN_x aperture sizes, which was accomplished by changing the lipid bilayer radius (R_{lipid}) in the model. In line with expectation, as we varied V_g, the ionic current remained unchanged for large bilayer sizes (R_{lipid} = 40, 20, and 10 nm). However, as the R_{lipid} value dropped below 10 nm (R_{lipid} = 5, 2, and 1 nm), we observed a gating behavior with enhanced ionic current at negative V_g and decreased current at positive V_g (Fig. 2A, B). Furthermore, we noticed that the higher currents at negative V_g were due to an increased cation flow, suggesting that gating also directly impacted the cation/anion selectivity of the device (Fig. 2A, inset). As a negative gate voltage made the channel surface potential more negative, it attracted more cations, which increased the overall ionic current in this cation selective channel. Positive gate voltages reduced the negative surface potential, lowering the cation current that dominated the conductance in this device. Despite the strength of the electric field at the CNTP increasing as R_{lipid} decreases (Fig. 2C and 2D), our simulations never showed gating factors higher than 10, indicating that reducing the lipid bilayer patch size alone was a poor way to obtain efficient gating.

Another, and potentially more important, parameter influencing gating in a CNTP device is the composition of the lipid membrane and its dielectric properties. We modeled these effects using different relative permittivity values for the inner and outer lipid bilayer regions. For these simulations we kept the bilayer size, R_{lipid}, constant at 20 nm. In the original condition, the relative permittivity of the outer regions, corresponding to the hydrophilic lipid head groups, was set to 3, while the permittivity of hydrophobic inner part was set to 1.[40] We examined various lipid membrane compositions by using different combinations of relative permittivity values for the inner and outer lipid regions, which we denote as *lipid(outer, inner, outer)* (Fig. 3A and S1). When the dielectric permittivity of

the outer regions was kept constant, higher inner permittivity values resulted in higher gating factors (Fig. 3B - E). A comparison of Fig. 3C, D and E shows that as the inner permittivity increases, the electric field starts to propagate much closer to the CNTP.

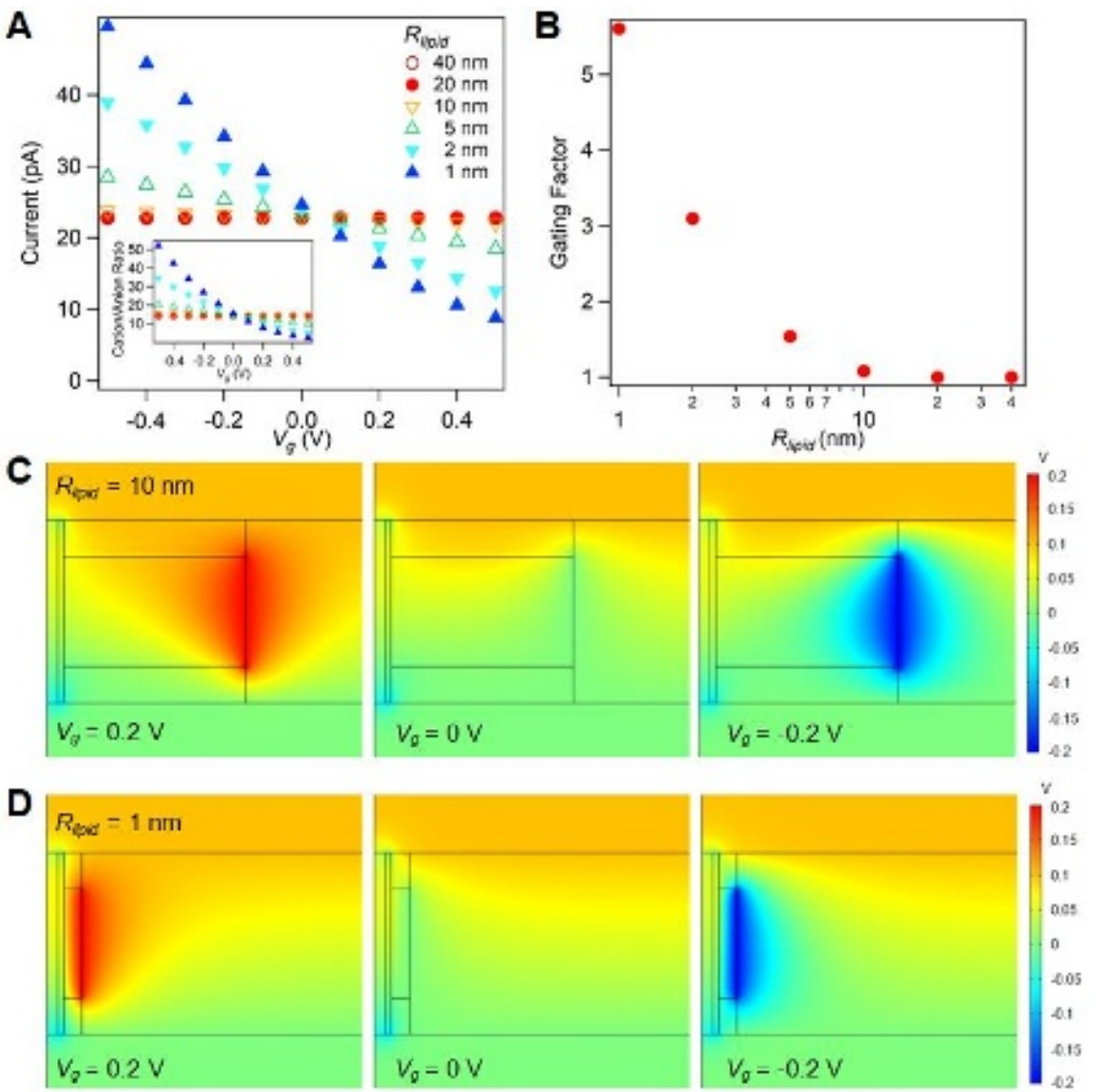

Figure 2. Lipid bilayer patch size and CNTP gating. (**A**) Ion current through the CNTP channel as a function of V_g at V_p = 0.1 V for R_{lipid} = 1, 2, 5, 10, 20, and 40 nm. Inset: Calculated cation/anion selectivity ratio. (**B**) Plot of the gating factor for different lipid patch sizes, R_{lipid}. (**C, D**) Electric potential distributions at V_p = 0.1 V for R_{lipid} = 10 nm (C) and 1 nm (D) calculated for V_g = 0.2 V (left), 0 V (center), and -0.2 V (right).

We obtained the highest gating factor values for the configurations where the inner region permittivity was high, and the outer region permittivity was low. This observation is not surprising, as in order to prevent field dissipation into the solution reservoirs and maintain high gating efficiency an ideal bilayer matrix must have outer lipid regions with low relative permittivity values (Fig. 3B). This effect is clearly observable by comparing the field distribution for *lipid(10,80,10)* (Fig. 3F) to *lipid(1,80,1)* (Fig. 3E), where the electric field in the former is much weaker and much closer to what was observed for the *lipid(1,10,1)* configuration. We have also investigated whether the change in the gating efficiency is driven by the absolute values of the bilayer matrix permittivity or the ratio of the permittivity values of the inner and outer region. We observed strong correlation between the calculated gating factor values and the absolute values of the permittivity of the inner bilayer region (Fig. S2A). In contrast, the correlation with the ratio of the inner and outer region permittivity was much weaker (Fig. S2B), indicating that absolute value of the permittivity of the inner region remains the dominant factor that determined gating efficiency. Overall, the gating factors improve from ca. 5x observed for *lipid(1,10,1)* to ca. 30x for *lipid(1,80,1)*. Although these gating factors are much lower than that the typical on/off ratios for solid-state transistors (10^7-10^9x), they are comparable to the gating factor values achievable using ionic field effect transistors, such as microfluidic transistors (5-100x).[41, 42]

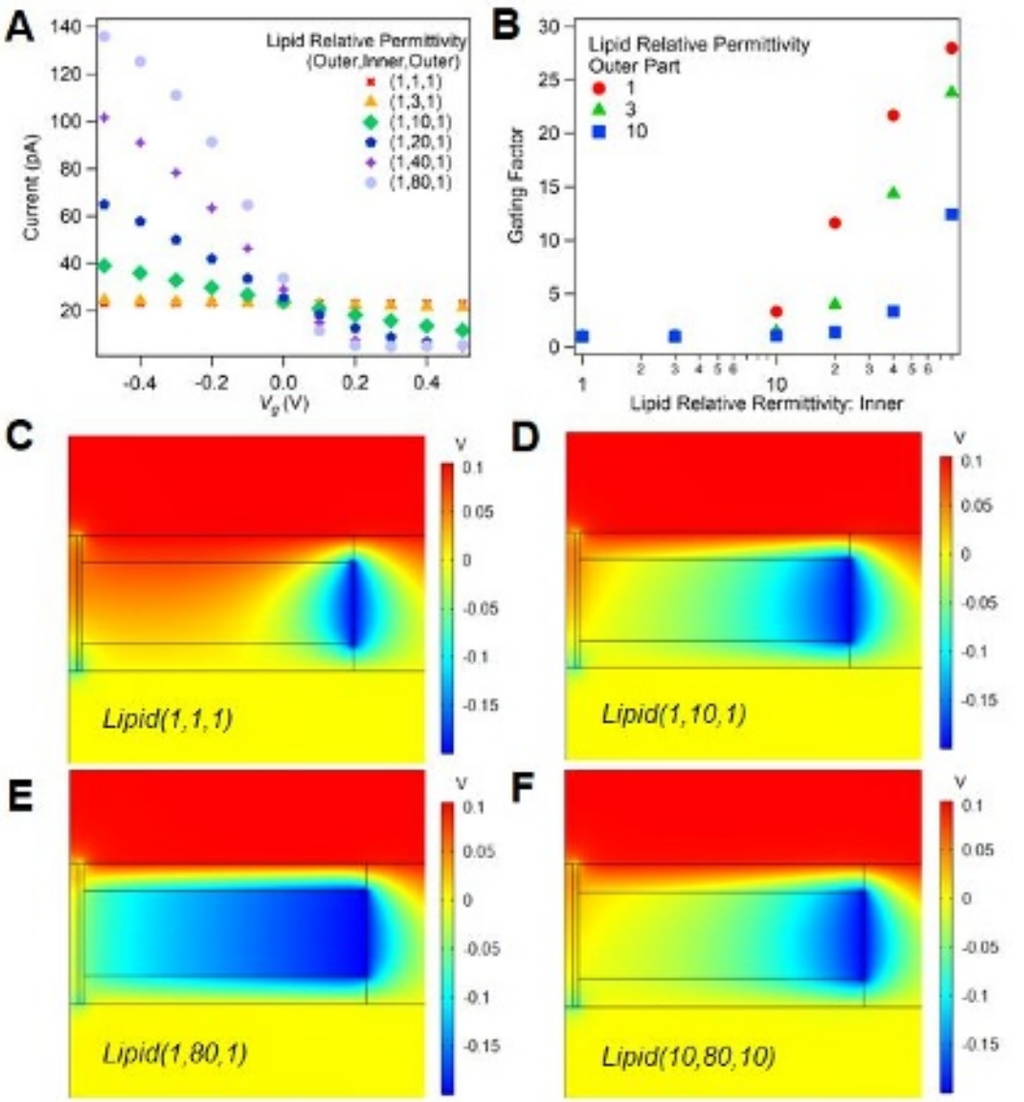

Figure 3. Lipid membrane dielectric properties and CNTP gating. (**A**) Calculated ionic current as a function of applied gate voltage, V_g, at V_p = 0.1 V. The outer lipid layer relative permittivity was set to be 1 and inner lipid relative permittivity values varied from 1 to 80 as indicated on the legend. (**B**) Calculated gating factors as a function of relative permittivity of both lipid outer and inner parts. (**C-F**) Surface electric potential distribution at V_p = 0.1 V and V_g = -0.2 V calculated for four lipid matrix compositions: *lipid(1,1,1)* (**C**), *lipid(1,10,1)* (**D**), *lipid(1,80,1)* (**E**), and *lipid(10,80,10)* (**F**).

Based on these results, we conclude that to maximize gating efficiency in a CNTP devices we need to use small bilayer patches with highly conductive inner regions and insulating outer regions. As fabricating SiN_x aperture devices with radii smaller than 20 nm is quite difficult, control of the bilayer composition represents a more attractive experimental

opportunity. A properly engineered lipid bilayer matrix also produces higher gating efficiencies even for a relatively large membrane size (R_{lipid} = 20 nm). What are the possible approaches to engineer such bilayer structures? Most lipid molecules have relative permittivity values around 1 to 3.[40] Lipid doping could produce more conductive lipid bilayers and researchers have shown that organic semiconducting materials or conductive polymers can be doped into lipid bilayer membranes, resulting in higher relative permittivity values;[37, 43, 44] two such examples include conjugating oligo-electrolytes into microbial membranes and inserting PEDOT-S into supported lipid membranes.[45, 46] An alternative approach for modulating the permittivity of the inner lipid region is to include a thin film of water in-between lipid layers, as done by Schibel *et al*.[47] This approach would enable the realization of the lipid composition *lipid(1,80,1)*, thus maximizing gating efficiency.

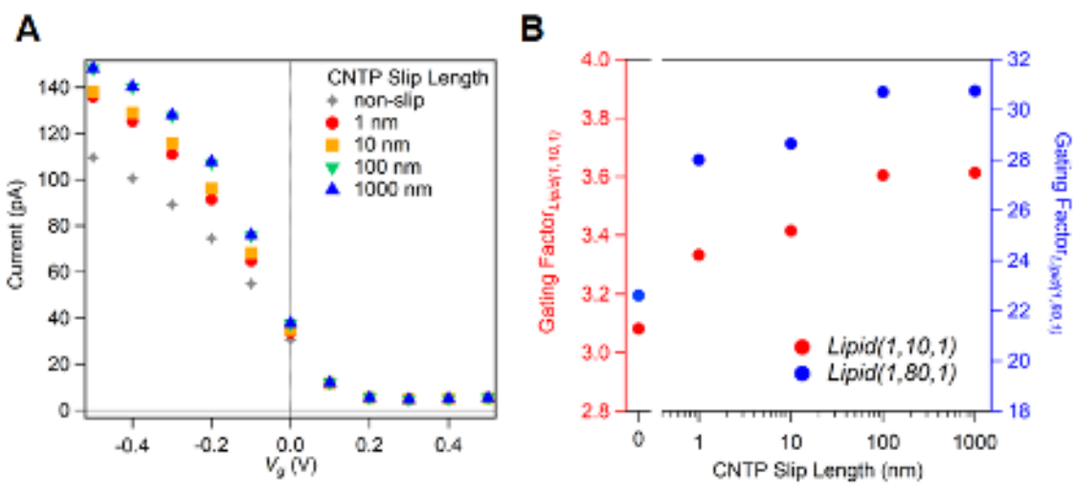

Figure 4. CNT slip length and CNTP gating. (**A**) Ionic current as a function of V_g for various CNTP slip length 0, 1, 10, 100, 1000 nm with *lipid(1,80,1)*. (**B**) The gating factor for different CNTP slip length with two lipid permittivity conditions: *lipid(1,80,1)* (blue, right axis) and *lipid(1,10,1)* (red, left axis). All simulations assumed R_{lipid} = 20 nm and V_p = 0.1 V.

Carbon nanotube properties and gating efficiency

Another important question is whether intrinsic properties of the CNTPs, such as their electronic nature and slip length, impact the gating characteristics of the final device.[27, 48] Slip length is an important parameter impacting both the electroosmotic flow

and ion transport through the CNTP. Intuitively, lower intrinsic friction for the transport should lead to more sensitivity to external gating. In our initial set of simulations we set the slip length to 1 nm to match the value derived from the experimental conductance measurements for d = 1.5 nm CNTPs.[20] However, several studies have suggested that the slip length may be much larger depending on factors such as CNT chirality or the presence of additional chemical moieties.[10] To study the effect of different CNTP slip lengths on gating, we compared the gating factor values obtained in our simulations for two lipid systems, *lipid(1,80,1)* (Fig. 4A) and *lipid(1,10,1)* (Fig. S3), with slip lengths ranging from 0 (non-slip) to 1000 nm. For both lipid systems, we obtained gating at all slip lengths, with a higher slip length producing a higher gating factor. However, this enhancement was very minimal, less than 10% (Fig. 4B), indicating that CNTP slip length does not significantly impact the CNTP gating efficiency, which is in agreement with the observation by Lucas *et al.* that creeping flow does not significantly impact the gating effect.[29]

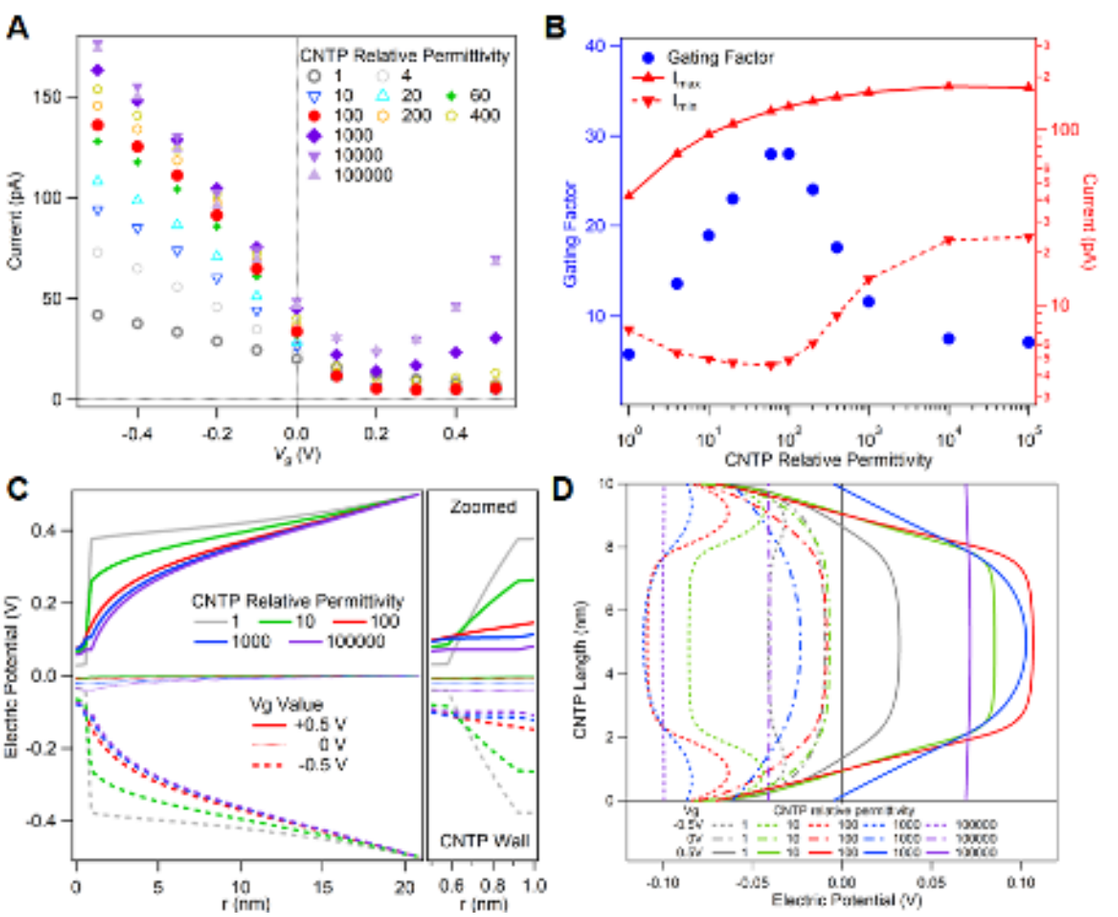

Figure 5. Electronic properties of CNTPs and CNTP gating. (**A**) Ionic current as a function of V_g for different CNTP relative permittivity values at V_p = 0.1 V. (**B**) Gating factors (left axis) and I_{max}, I_{min} (right axis) as a function of CNTP relative permittivity values. (**C**) Electrical potential profiles showing propagation of the gate electrode potential (r = 20.92 nm indicates electrode location and r = 0 nm corresponds to the center of the channel) for representative CNTP relative permittivity values: 1, 10, 100, 100000 at V_p = 0 V and gate voltage values varied as V_g = 0.5, 0, -0.5 V. Zoomed-in area: Comparison of the electric potential profiles within the CNTP wall region (r = 0.58 to 0.92 nm). (**D**). Profiles of the electric potential distribution along the CNTP wall (r = 0.58 nm) from the bottom (length = 0 nm) to the top of the CNTP (length = 10 nm) for representative CNTP relative permittivity values at V_p = 0 V and gate voltage values varied as V_g = 0.5, 0, -0.5 V. All simulations assumed R_{lipid} = 20 nm with *lipid(1,80,1)*.

CNTs can be semiconducting, semi-metallic, or metallic in nature depending on the nanotube structure (chirality).[49] Difficulties associated with obtaining chirally pure samples mean that, to date, many experimental studies use CNTs that are a mix of both metallic and semiconducting nanotubes and, as a result, permittivity values are unknown. However, as chirality sorting techniques continue to improve, an increase in the availability of pure semiconducting and metallic samples means that devices can be constructed using nanotubes with more well-defined electronic properties.[50-53] We modeled CNTPs with different electronic structures by assigning different relative permittivity values to the CNTP walls (Fig. 5A and S4) and then calculated the impact this had on the ion transport. Relative permittivity values of 30-100 corresponded to semiconducting nanotubes, while values above 1000 represented pure metallic nanotubes.[54] In the absence of an applied gate voltage (V_g = 0 V), metallic nanotubes had higher ionic currents than their semiconducting counterparts, in agreement with previous experimental observations.[27, 48] We attributed this phenomenon to the more effective delocalization of the negative entrance charge along the metallic CNTP (Fig. 5D and S5), which led to higher accumulation of cations inside the channel (Fig. S6) and thus to higher overall conductance.

The other notable observation was that the gating efficiency did not monotonically increase over different CNTP relative permittivity values (Fig. 5B). The highest gating factor values appeared at a CNTP permittivity value around 100. After examining the underlying values impacting the gating factor, I_{max} and I_{min}, it became clear to us that the distribution of the gating factor values was strongly impacted by the variations in I_{min} (Fig. 5B). While I_{max} continuously increased with increasing permittivity values, the I_{min} values

showed a distinct minimum at the permittivity value range corresponding to semiconducting nanotubes.

Electric potential distributions (Fig. 5C, D) provide strong clues as to why these nanotubes were the most effective at shutting down the ion current under positive applied potential. Negative entrance charges remained localized in a semiconducting CNTP even in the presence of external fields (Fig. 5D), and thus could provide an effective barrier for anion transport. In addition, semiconducting nanotubes allowed the electric field to propagate into the channel (Fig 5D, red lines), creating an effective barrier for cation transport at positive V_g values, as evidenced by the low cation concentration in the middle of the nanotube (Fig. S6). As the result, both cation and anion transport was suppressed at positive V_g values and the overall ion current through the channel was minimized. In insulating CNTPs (Fig. 5C, D, gray lines) the electric field applied by the gate electrode could not effectively penetrate into the channel, allowing cation flow even at positive gate voltages and producing higher I_{min} current values. Metallic CNTPs, on the contrary, were quite efficient in propagating the gating field into the middle of the channel and effectively shutting down the cation current. However, they were also very effective in delocalizing charge, meaning that an external gate voltage was able to alter the potential over the entire nanotube (Fig 5D, purple lines). As a result, when we applied a sufficiently positive gate voltage to the metallic nanotube in the simulation, we were able to reverse the effective charge, repelling the cations. However, this charge reversal simultaneously reduced the barrier to anion transport, leading to anions becoming the primary charge carrier. Indeed, the increase in total current observed at high positive V_g for permittivity values above 1000 was due to anion flow, confirming this hypothesis (Fig. 5A, S4 and S6). Based on these findings, we conclude that, in order to achieve optimum gating performance, an ideal CNTP-based gate device should incorporate semiconducting CNTs.

Conclusions

In this work, we used COMSOL simulations to investigate gating of carbon nanotube porins. Our results showed that efficient gating can be achieved in a device with an individual CNTPs embedded within a thin membrane matrix. Our simulations show that the best gating occurs in a device that consists of a semiconducting CNTP (with

permittivity values *ca.* 80-100) inserted into a thin membrane with a highly polarizable or conductive interior, which potentially could be accomplished by doping the lipid bilayer. We further demonstrated that the gate electric field can strongly affect the surface charge distribution of the CNTP channel, and that the extent by which this occurs is dependent on the nanotube's electronic nature. The results from our model demonstrate that electrostatic gating is impacted directly by the ion distribution and cation/anion selectivity. Additional factors, such as changes in ion mobility and hydration/dehydration energy, can play important roles in the gating effect mechanisms for ion transport in confined spaces.[55, 56] However, a COMSOL model does not account for these effects and capturing them would require molecular dynamics simulations. This electrostatic gating mechanism can be used to control the ionic flow and selectivity in the device. Our simulations show that these devices can control ion transport through the CNTP channel using gate voltages that are well within a bio-compatible range of values, indicating that these concepts can be used for real-world bioelectronics applications.

Data Availability

The data that support the findings of this study are openly available in Figshare.com at http://doi.org/10.6084/m9.figshare.14535975.

Supplementary Materials

Supplementary Materials section contains additional details for COMSOL modeling, and additional results from the simulations of the role of lipid composition, CNTP slip lengths, and CNTP relative permittivity on the surface electric potential distributions, ion concentration profiles and ion conductance.

Acknowledgements

This work was supported as part of the Center for Enhanced Nanofluidic Transport (CENT), an Energy Frontier Research Center funded by the U.S. Department of Energy, Office of Science, Basic Energy Sciences under award no. DE-SC0019112. We thank Pedro de Souza (MIT) for discussions about COMSOL modeling. Work at the Lawrence Livermore National Laboratory was performed under the auspices of the U.S. Department of Energy under Contract DE-AC52-07NA27344.

References

1. J. R. Werber, C. O. Osuji and M. Elimelech, Nat. Rev. Mater. **1** (5), 16018 (2016).
2. Z. Li, Y. Li, Y.-C. Yao, F. Aydin, C. Zhan, Y. Chen, M. Elimelech, T. A. Pham and A. Noy, ACS Nano **14** (5), 6269-6275 (2020).
3. R. Epsztein, R. M. DuChanois, C. L. Ritt, A. Noy and M. Elimelech, Nature Nanotechnology (2020).
4. K. Xiao, L. Jiang and M. Antonietti, Joule **3** (10), 2364-2380 (2019).
5. J. S. Cameron, *A history of the treatment of renal failure by dialysis*. (Oxford University Press Oxford, 2002).
6. L. Fumagalli, A. Esfandiar, R. Fabregas, S. Hu, P. Ares, A. Janardanan, Q. Yang, B. Radha, T. Taniguchi, K. Watanabe, G. Gomila, K. S. Novoselov and A. K. Geim, Science **360** (6395), 1339-1342 (2018).
7. K. Gopinadhan, S. Hu, A. Esfandiar, M. Lozada-Hidalgo, F. C. Wang, Q. Yang, A. V. Tyurnina, A. Keerthi, B. Radha and A. K. Geim, Science **363** (6423), 145-148 (2019).
8. S. Joseph and N. R. Aluru, Nano Lett. **8** (2), 452-458 (2008).
9. R. H. Tunuguntla, R. Y. Henley, Y. C. Yao, T. A. Pham, M. Wanunu and A. Noy, Science **357** (6353), 792-796 (2017).
10. E. Secchi, S. Marbach, A. Nigues, D. Stein, A. Siria and L. Bocquet, Nature **537** (7619), 210-213 (2016).
11. G. Hummer, J. C. Rasaiah and J. P. Noworyta, Nature **414** (6860), 188-190 (2001).
12. Y. Li, Z. Li, F. Aydin, J. Quan, X. Chen, Y. C. Yao, C. Zhan, Y. Chen, T. A. Pham and A. Noy, Science advances **6** (38) (2020).
13. J. Feng, M. Graf, K. Liu, D. Ovchinnikov, D. Dumcenco, M. Heiranian, V. Nandigana, N. R. Aluru, A. Kis and A. Radenovic, Nature (2016).
14. A. Horner, F. Zocher, J. Preiner, N. Ollinger, C. Siligan, S. A. Akimov and P. Pohl, Science advances **1** (2), e1400083 (2015).
15. L. Bocquet, Nature materials **19** (3), 254-256 (2020).
16. K. V. Agrawal, S. Shimizu, L. W. Drahushuk, D. Kilcoyne and M. S. Strano, Nature nanotechnology **12** (3), 267-273 (2017).
17. E. Secchi, A. Nigues, L. Jubin, A. Siria and L. Bocquet, Phys. Rev. Lett. **116** (15), 154501 (2016).
18. P. M. Biesheuvel and M. Z. Bazant, Physical review. E **94** (5-1), 050601 (2016).
19. Y. Noh and N. R. Aluru, ACS Nano **14** (8), 10518-10526 (2020).
20. Y.-C. Yao, A. Taqieddin, M. A. Alibakhshi, M. Wanunu, N. R. Aluru and A. Noy, ACS Nano **13** (11), 12851-12859 (2019).
21. N. Kavokine, R. R. Netz and L. Bocquet, Annu. Rev. Fluid Mech. **53** (1), null (2021).
22. A. Fang, K. Kroenlein, D. Riccardi and A. Smolyanitsky, Nat. Mater. **18** (1), 76 (2019).
23. A. Marcotte, T. Mouterde, A. Niguès, A. Siria and L. Bocquet, Nat. Mater. **19** (10), 1057-1061 (2020).
24. S. Tornroth-Horsefield, Y. Wang, K. Hedfalk, U. Johanson, M. Karlsson, E. Tajkhorshid, R. Neutze and P. Kjellbom, Nature **439** (7077), 688-694 (2006).

25. S. C. Cannon, in *Encyclopedia of the Neurological Sciences (Second Edition)*, edited by M. J. Aminoff and R. B. Daroff (Academic Press, Oxford, 2014), pp. 747-751.
26. S. Faucher, N. Aluru, M. Z. Bazant, D. Blankschtein, A. H. Brozena, J. Cumings, J. Pedro de Souza, M. Elimelech, R. Epsztein and J. T. Fourkas, The Journal of Physical Chemistry C **123** (35), 21309-21326 (2019).
27. P. Pang, J. He, J. H. Park, P. S. Krstic and S. Lindsay, ACS Nano **5** (9), 7277-7283 (2011).
28. A. Marcotte, T. Mouterde, A. Nigues, A. Siria and L. Bocquet, Nature materials **19** (10), 1057-1061 (2020).
29. R. A. Lucas and Z. S. Siwy, ACS Appl. Mater. Interfaces **12** (50), 56622-56631 (2020).
30. R. Karnik, R. Fan, M. Yue, D. Li, P. Yang and A. Majumdar, Nano Lett. **5** (5), 943-948 (2005).
31. R. Karnik, K. Castelino and A. Majumdar, Appl. Phys. Lett. **88** (12), 123114 (2006).
32. W. Guan, R. Fan and M. A. Reed, Nature communications **2** (1), 506 (2011).
33. G. Sun, S. Senapati and H. C. Chang, Lab Chip **16** (7), 1171-1177 (2016).
34. J. Geng, K. Kim, J. Zhang, A. Escalada, R. Tunuguntla, L. R. Comolli, F. I. Allen, A. V. Shnyrova, K. R. Cho, D. Munoz, Y. M. Wang, C. P. Grigoropoulos, C. M. Ajo-Franklin, V. A. Frolov and A. Noy, Nature **514** (7524), 612-615 (2014).
35. R. H. Tunuguntla, A. Escalada, A. F. V and A. Noy, Nature protocols **11** (10), 2029-2047 (2016).
36. C.-Y. Lin, P.-H. Wong, P.-H. Wang, Z. S. Siwy and L.-H. Yeh, ACS Appl. Mater. Interfaces **12** (2), 3198-3204 (2020).
37. T. Ma, X. Feng, T. Ohori, R. Miyata, D. Tadaki, D. Yamaura, T. Deguchi, M. Komiya, K. Kanomata, F. Hirose, M. Niwano and A. Hirano-Iwata, ACS omega **4** (19), 18299-18303 (2019).
38. X. Kang, M. A. Alibakhshi and M. Wanunu, Nano Lett. **19** (12), 9145-9153 (2019).
39. T. Gutsmann, T. Heimburg, U. Keyser, K. R. Mahendran and M. Winterhalter, Nature protocols **10** (1), 188-198 (2015).
40. W. Huang and D. G. Levitt, Biophys J **17** (2), 111-128 (1977).
41. S. M. Sze and K. K. Ng, *Physics and properties of semiconductors—A review*. (2006).
42. S.-W. Nam, M. J. Rooks, K.-B. Kim and S. M. Rossnagel, Nano Lett. **9** (5), 2044-2048 (2009).
43. P. E. Schwenn, P. L. Burn and B. J. Powell, Org. Electron. **12** (2), 394-403 (2011).
44. H. Sun, S. Ryno, C. Zhong, M. K. Ravva, Z. Sun, T. Körzdörfer and J.-L. Brédas, J. Chem. Theory Comput. **12** (6), 2906-2916 (2016).
45. P. K. Johansson, D. Jullesson, A. Elfwing, S. I. Liin, C. Musumeci, E. Zeglio, F. Elinder, N. Solin and O. Inganas, Sci Rep **5**, 11242 (2015).
46. A. W. Thomas, L. E. Garner, K. P. Nevin, T. L. Woodard, A. E. Franks, D. R. Lovley, J. J. Sumner, C. J. Sund and G. C. Bazan, Energy & Environmental Science **6** (6), 1761-1765 (2013).
47. A. E. Schibel, E. C. Heider, J. M. Harris and H. S. White, J Am Chem Soc **133** (20), 7810-7815 (2011).

48. L. Liu, C. Yang, K. Zhao, J. Li and H.-C. Wu, Nature communications **4** (1), 2989 (2013).
49. *Carbon Nanotubes: Synthesis, Structure, Properties, and Applications*. (Springer, 2001).
50. J. A. Fagan, Nanoscale Adv. **1** (9), 3307-3324 (2019).
51. H. Li, G. Gordeev, O. Garrity, N. A. Peyyety, P. B. Selvasundaram, S. Dehm, R. Krupke, S. Cambré, W. Wenseleers, S. Reich, M. Zheng, J. A. Fagan and B. S. Flavel, ACS Nano **14** (1), 948-963 (2020).
52. H. Li, G. Gordeev, O. Garrity, S. Reich and B. S. Flavel, ACS Nano **13** (2), 2567-2578 (2019).
53. H. J. An, S. Kim, H. Seo, P. J. Yoo and W.-J. Kim, Appl. Surf. Sci. **508**, 145258 (2020).
54. W. Lu, D. Wang and L. Chen, Nano Lett. **7** (9), 2729-2733 (2007).
55. A. Esfandiar, B. Radha, F. C. Wang, Q. Yang, S. Hu, S. Garaj, R. R. Nair, A. K. Geim and K. Gopinadhan, Science **358** (6362), 511-513 (2017).
56. C. Duan and A. Majumdar, Nat Nanotechnol **5** (12), 848-852 (2010).

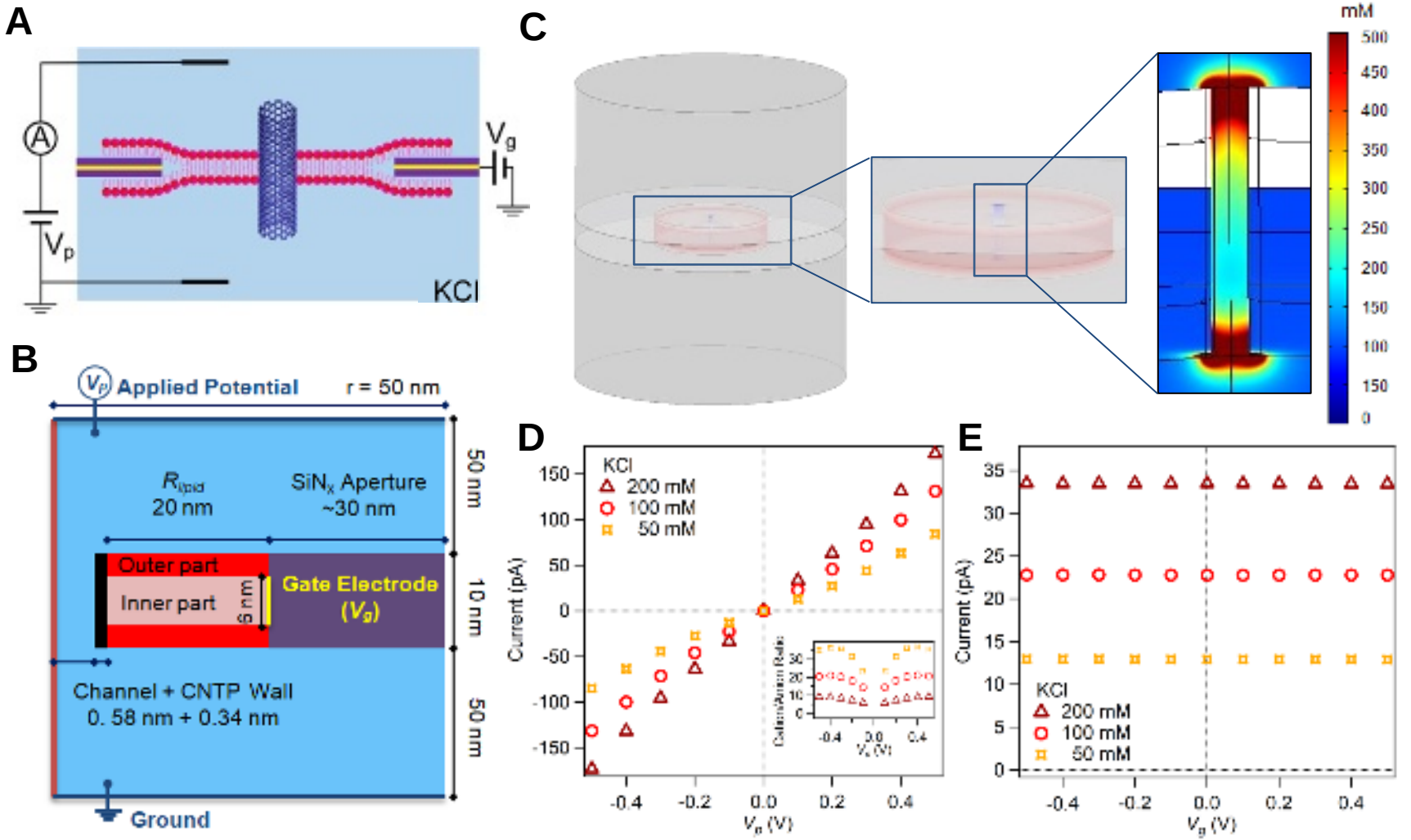
A
KCl
V_g
V_p
B
V_p Applied Potential
r = 50 nm
R_{pore}
20 nm
SiN_x Aperture
~30 nm
Outer part
Inner part
5 nm
Gate Electrode
(V_g)
Channel + CNTP Wall
0. 58 nm + 0.34 nm
Ground
50 nm
10 nm
50 nm
C
mM
500
450
400
350
300
250
200
150
100
150
0
D
KCl
200 mM
100 mM
50 mM
Current (pA)
V_p (V)
E
KCl
200 mM
100 mM
50 mM
Current (pA)
V_g (V)

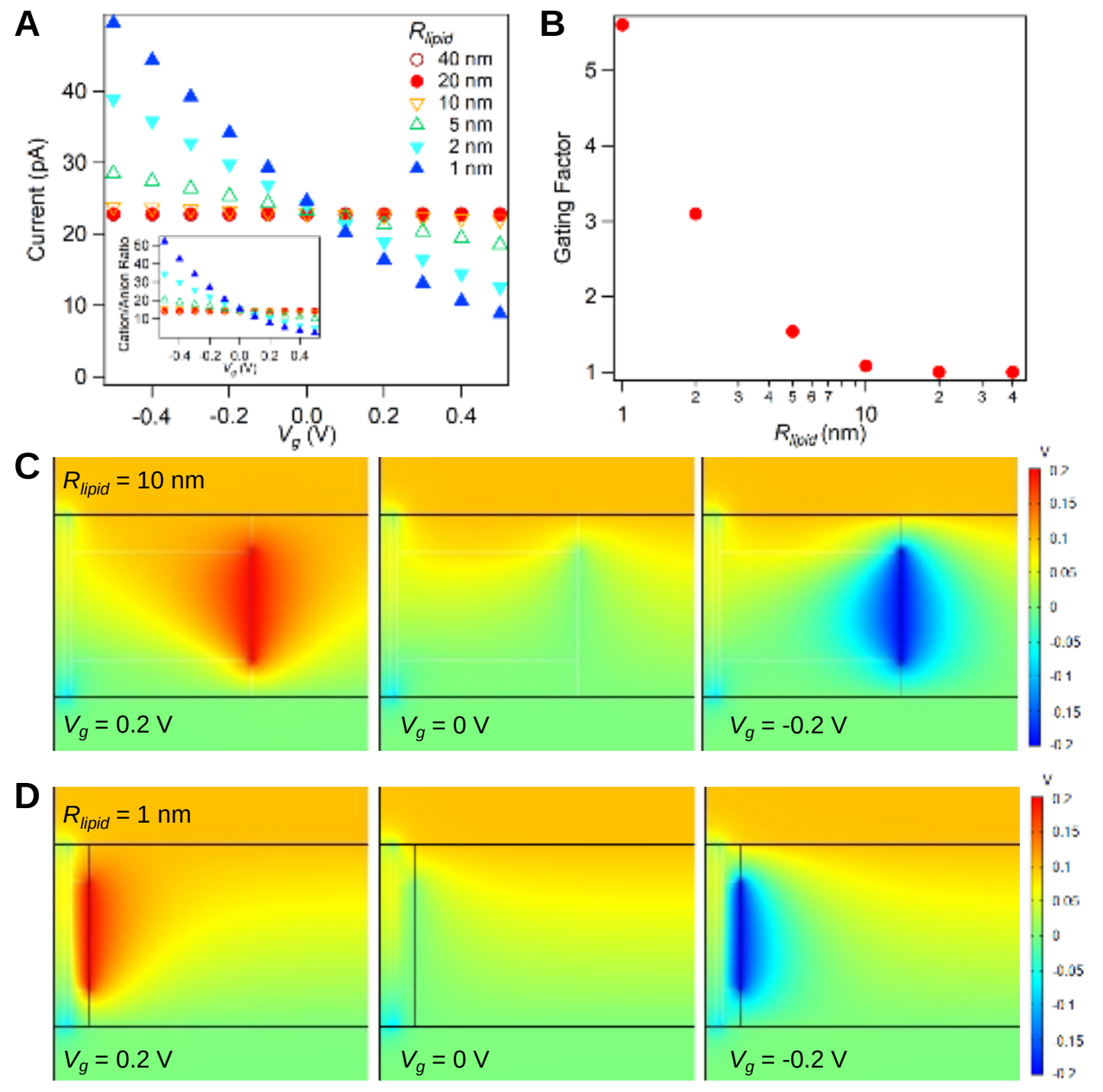
A
Current (pA)
V_g (V)
R_{lipid}
40 nm
20 nm
10 nm
5 nm
2 nm
1 nm
Cation/Anion Ratio
B
Gating Factor
R_{lipid} (nm)
C
R_{lipid} = 10 nm
V_g = 0.2 V
V_g = 0 V
V_g = -0.2 V
V
D
R_{lipid} = 1 nm
V_g = 0.2 V
V_g = 0 V
V_g = -0.2 V
V

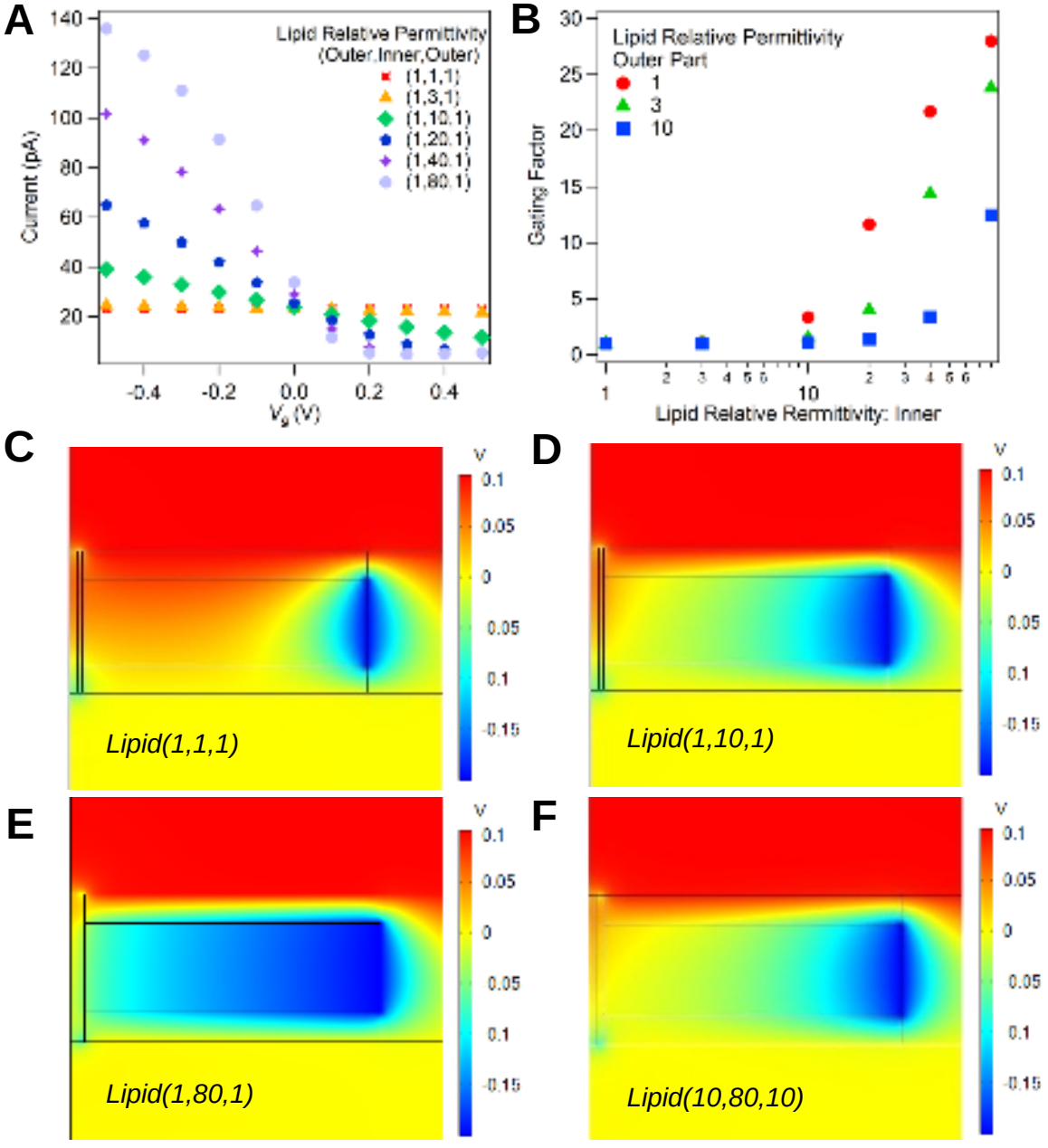
A
Lipid Relative Permittivity
(Outer,Inner,Outer)
(1,1,1)
(1,3,1)
(1,10,1)
(1,20,1)
(1,40,1)
(1,80,1)
Current (pA)
V_g (V)
B
Lipid Relative Permittivity
Outer Part
1
3
10
Gating Factor
Lipid Relative Permittivity: Inner
C
Lipid(1,1,1)
D
Lipid(1,10,1)
E
Lipid(1,80,1)
F
Lipid(10,80,10)
V

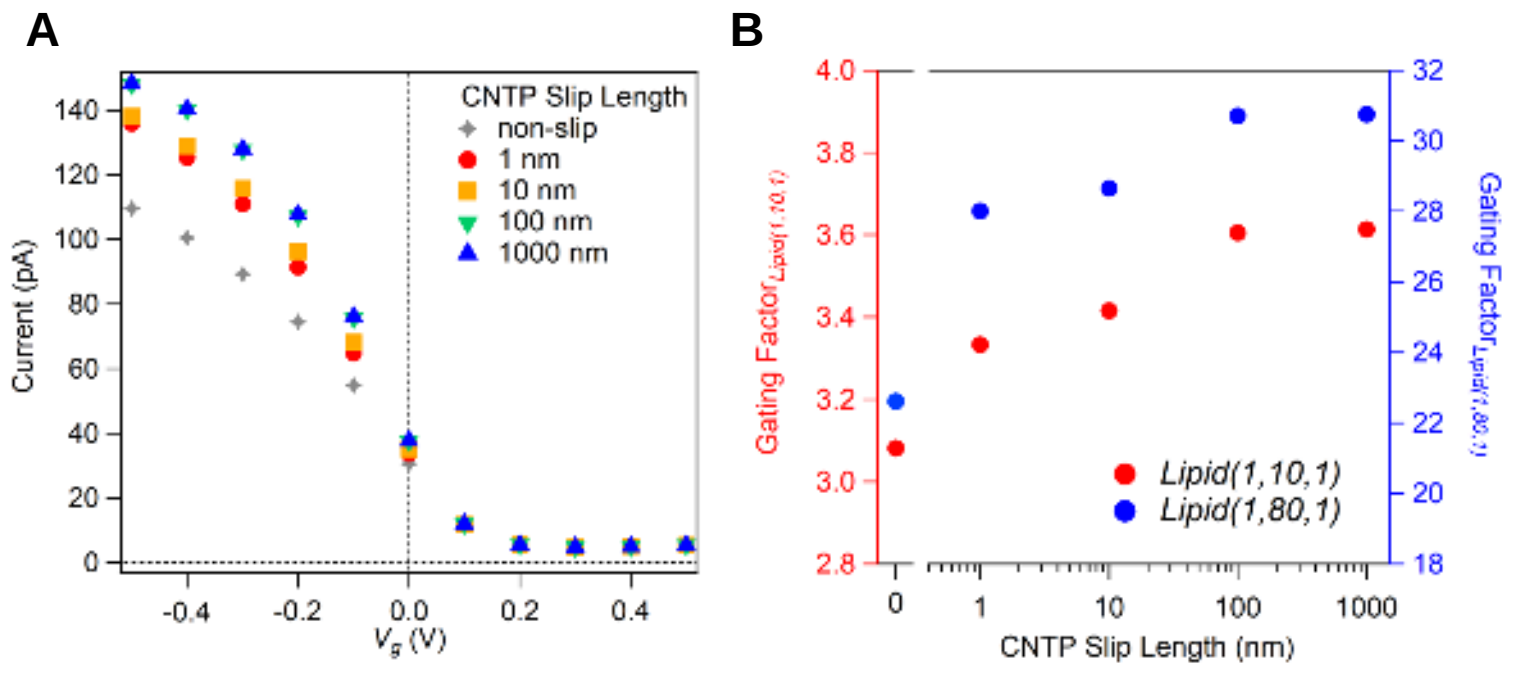
A
B
CNTP Slip Length
non-slip
1 nm
10 nm
100 nm
1000 nm
Current (pA)
V_g (V)
Gating Factor$_{Lipid(1,10,1)}$
Gating Factor$_{Lipid(1,80,1)}$
Lipid(1,10,1)
Lipid(1,80,1)
CNTP Slip Length (nm)

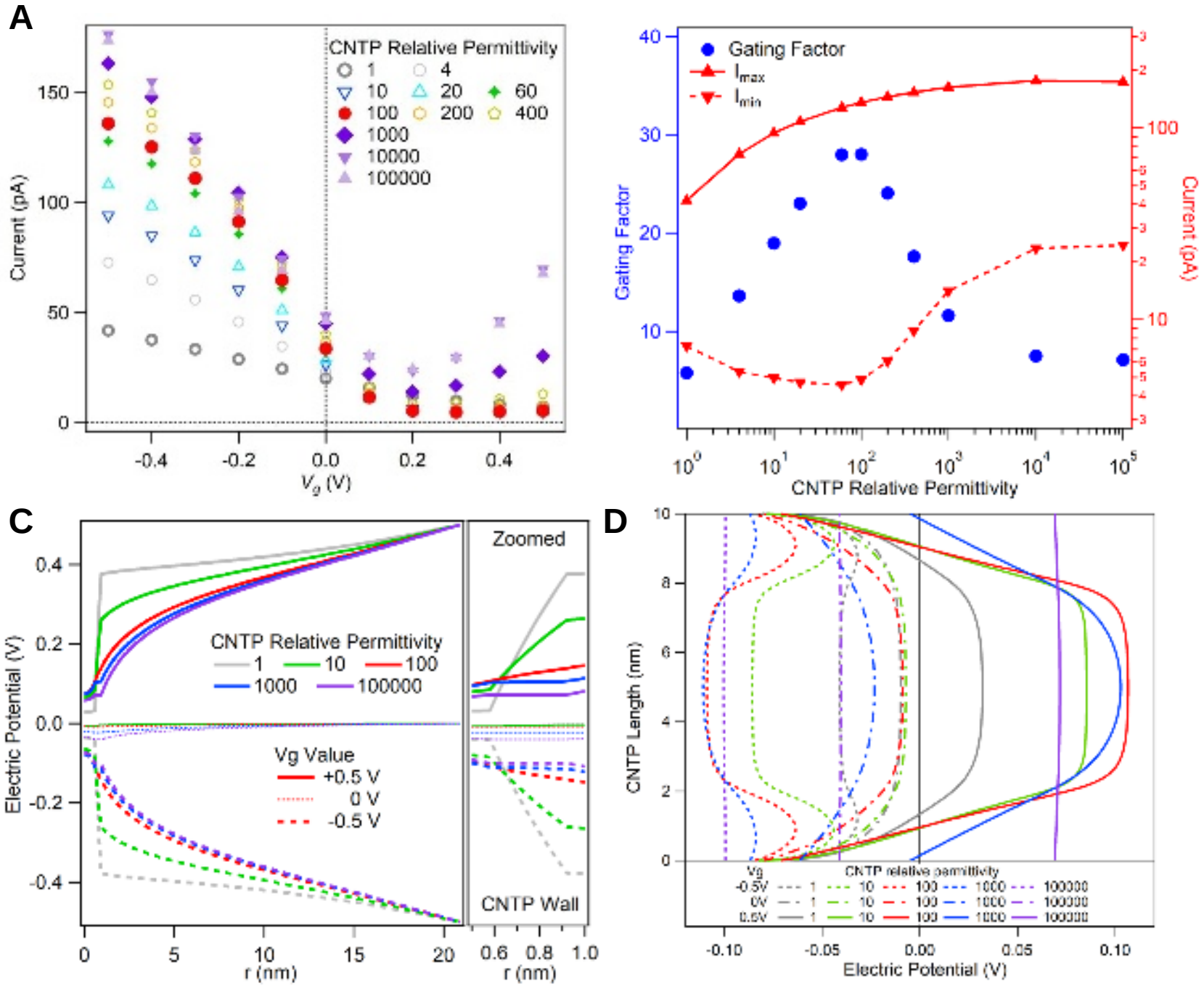
A
CNTP Relative Permittivity
1
4
10
20
60
100
200
400
1000
10000
100000
Current (pA)
V_g (V)
Gating Factor
I_{max}
I_{min}
Gating Factor
Current (pA)
CNTP Relative Permittivity
C
Zoomed
CNTP Relative Permittivity
Vg Value
+0.5 V
0 V
-0.5 V
Electric Potential (V)
CNTP Wall
r (nm)
r (nm)
D
CNTP Length (nm)
Vg
CNTP relative permittivity
Electric Potential (V)